JOURNAL OF PROPULSION AND POWER
Vol. 26, No. 2, March–April 2010

Combustion Dynamics and Stability of a Fuel-Rich Gas Generator

Seonghyeon Seo,* Seong-Ku Kim,† and Hwan-Seok Choi‡
Korea Aerospace Research Institute, 305-333 Daejeon, Republic of Korea

DOI: 10.2514/1.46568

The dynamic characteristics of fuel-rich combustion have been studied using an experimental combustor simulating a gas generator for a liquid rocket engine. The combustor burns liquid oxygen and fuel (Jet A-1) at a mixture ratio of about 0.32 and a chamber pressure ranging from 4.10 to 7.24 MPa, which covers subcritical to supercritical pressures of oxygen. For the investigation of combustion dynamics, pressure fluctuation measurements using piezoelectric sensors have been a major probe throughout the present study. Two different types of injector heads equipped with biliquid swirl coaxial injectors and either a short nozzle or a turbine manifold nozzle have been used in the study. Fuel-rich combustion of both injector heads with the short nozzle revealed pressure pulsation at frequencies of about 128 Hz, which attenuates along with an increase of a chamber pressure. Combustion tests with the turbine manifold nozzle conducted at chamber pressures lower than the oxygen critical pressure showed combustion instabilities at a frequency of 330 Hz, which has been identified as a longitudinal resonant mode by a linear acoustic analysis. The combustion instabilities seem to be induced by inherent pressure fluctuations from the biliquid swirl coaxial injector when the chamber pressure is below the oxygen critical pressure.

Nomenclature

A	=	cross-sectional area, m^2
a	=	speed of sound, m/s
c^*	=	characteristic velocity defined as $(p_c A_{\text{th}})/(\dot{m}_o + \dot{m}_f)$, m/s
d	=	diameter, mm
f	=	frequency, Hz
$\dot{m}$	=	mass flow rate, kg/s
n	=	number of tangential entry
p	=	pressure, MPa
Q	=	volume flow rate, m^3/s
T	=	temperature, K
η	=	damping ratio
$\Delta()$	=	difference in quantity
Π	=	transfer function defined as in Eq. (1)
$()'$	=	fluctuating quantity

Subscripts

c	=	chamber
cr	=	critical condition
f	=	fuel
inj	=	injector
n	=	nozzle
o	=	oxygen
oo	=	outer section of oxidizer post
rms	=	root mean square
s	=	swirl chamber
t	=	tangential entry
th	=	nozzle throat

Received 31 July 2009; revision received 22 December 2009; accepted for publication 28 December 2009.

*Senior Researcher, Combustion Chamber Department, 115 Gwahangno Yuseong; sxs223@kari.re.kr.

†Senior Researcher, Combustion Chamber Department, 115 Gwahangno Yuseong.

‡Head, Combustion Chamber Department, 115 Gwahangno Yuseong.

I. Introduction

A LIQUID rocket engine (LRE) requires a propellant supply system. Propellants can be supplied by a turbopump or a propellant tank pressurized with inert gas. A turbopump consisting of pumps and turbines requires a high-pressure gas to drive its turbines. A powerpack of a bipropellant LRE adopting a simple open cycle employs a gas generator that burns propellants at oxidizer- or fuel-rich conditions, as described in Fig. 1 [1]. A fuel-rich combustion technique has been generally accepted and widely practiced because combustion gases of an oxidizer-rich gas generator constitute a severe oxidizing environment on metal parts of hardware [2]. A bipropellant fuel-rich gas generator operates at very low mixture ratios and introduces a thermochemically unbalanced combustion condition. Because of a fuel-rich combustion environment, product gas from a gas generator manifests a relatively low temperature compared with that from a thrust chamber.

Major objectives for the successful development of a gas generator involve stable combustion, uniformly distributed gas temperature, and durable hardware satisfying the lifetime requirement. Among these design issues, the dynamic characteristics of fuel-rich combustion have become a major interest in the present study. A fuel-rich combustion technique has been used for producing high-pressure gas because the advent of a bipropellant LRE. Even with such a long period of practical usage of this kind of a gas-generating device, detailed information regarding fuel-rich combustion dynamic characteristics has been lacking in the public domain.

Relatively well-documented information regarding the development of a fuel-rich gas generator can be found from the development processes of a LRE called FASTRAC [3]. During the development combustion tests, Nesman and Dennis [4] observed that a gas generator equipped with fuel-oxidizer-fuel impinging injectors using liquid oxygen (LOx) and kerosene, that is, RP-1, showed low-frequency buzzing at off-nominal operating conditions with a power level of 45% and a mixture ratio of 0.36. The superior performance of a triplet impinging injector to a like-on-like doublet impinging injector with regard to combustion stability resistance had been shown by Heubner [5] through fuel-rich LOx/RP-1 hot-fire testing. Mah [6] conducted a series of combustion tests using a gas generator with like-on-like injectors fueled by nitrogen tetroxide and Aerozine 50. Pressure fluctuations increased as the mixture ratio was lowered. The worst cases were the ones in which the ratio of the pressure fluctuations to the chamber pressure was more than 20%. The level of

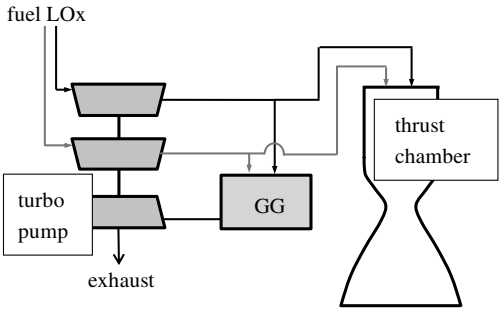

Fig. 1 Schematic of an open-cycle liquid rocket engine with a gas generator (GG).

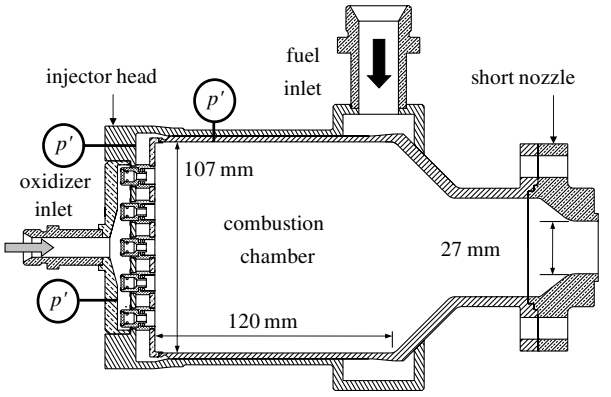

Fig. 2 Cross-sectional view of a regenerative fuel-rich combustor equipped with a short sonic nozzle for simulating turbine inlets.

the pressure fluctuations was reduced with the increase of the chamber pressure from 2.1 to 4.3 MPa at the same mixture ratio. Zurbach et al. [7] encountered strong low-frequency instability during their combustion tests of a fuel-rich LOx/liquid methane preburner. They concluded that the low-frequency instability had originated from a low-pressure drop in the methane line and that for stable operation the ratio of line pressure drop to the chamber pressure should be larger than 7%. With regard to the stability assessment of fuel-rich combustion, Fournet et al. [8] applied artificial pulsing devices to perturb the pressure field of a LOx/hydrogen gas generator operating at about 10 MPa and observed that the damping times ranged between 6 and 10 ms, which indicates stable combustion for the conditions tested.

To achieve uniform temperature distribution, a coaxial injector has been considered as the best choice in the present study because it shows axisymmetric distribution of the mass flux and mixture ratio [9]. Meanwhile, a coaxial injector with swirl flow provides unique dynamic characteristics in its injecting flow due to swirling motion. Sivakumar and Raghunandan [10] experimentally studied the atomization of biliquid swirl coaxial injectors and concluded that the merging of liquid sheets before disintegration results in the increase of the mean diameter of the global spray by 40–50% and that the enhancement of swirl intensity due to an increased flow rate improves the atomization quality of the spray. Soltani et al. [11] also conducted cold flow tests of biliquid swirl coaxial injectors. They obtained the interesting result that the velocity field of the combined spray is strongly affected by the Reynolds number change of the inner spray rather than that of the outer one, and that the outer spray Reynolds number change does not greatly affect the Sauter mean diameter of the droplets of the combined spray at a fixed inner spray Reynolds number. A similar cold flow study by Kim et al. [12] also observed that the inner spray effects are greater than those of the outer spray on breakup length variations. They had drawn the conclusion that the mixing of inner and outer sprays in the inside of an injector can impact spray characteristics, which enhances mixing.

The main objective of the present study is to understand the dynamic characteristics of fuel-rich combustion associated with differences in injector and chamber configurations along with chamber pressure variations from subcritical to supercritical conditions. Experimental approaches to characterize fuel-rich combustion dynamics included the measurements of pressure fluctuations employing two different types of biliquid swirl coaxial injectors with each individual injector layout and either a short nozzle or a turbine manifold nozzle. Moreover, a numerical acoustic analysis has been carried out to identify the acoustic modes occurring in the assembly of the combustor and the turbine manifold.

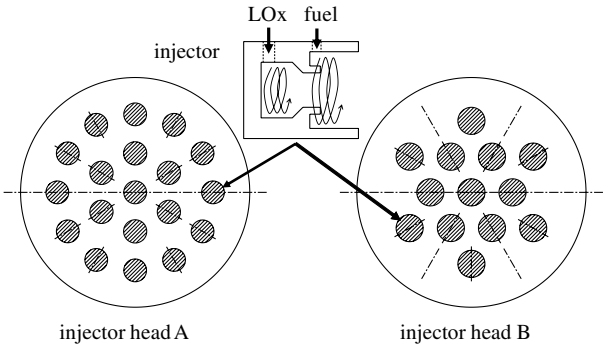

Fig. 3 Injector layouts of two injector heads and a cross-sectional schematic of a swirl coaxial injector.

II. Experimental Setup

A. Injector Heads

The present experimental combustor burns LOx and kerosene (Jet A-1) as propellants. The hardware itself consists of an injector head, a combustion chamber with a contraction section, and a nozzle section as illustrated in Fig. 2. Its subcomponents were all welded together except for an interchangeable nozzle. To acquire optimum designs of test hardware, a number of different pieces of hardware had been designed and manufactured for the series of preliminary combustion tests. Finally, a couple of injector heads were selected as presented in Fig. 3. One of the injector heads (injector head A) has a concentric layout of injectors with two radial rows and the other (injector head B) a layout of equidistant injectors.

Throughout the preliminary tests, the performance of the selected injector heads proved to satisfy the basic functional requirements for the present research. They all successfully operated at actual combustion conditions without physical failure or thermal damage on the injector face.

Each of the injector heads employs its own design of a biliquid swirl coaxial injector. The basic schematic of the injectors is shown in the middle of Fig. 3. Through the center post of the coaxial injector, oxidizer discharges and its spray sheet impinges on an outer fuel film inside the injector before exiting to the combustion chamber. As listed in Table 1, the coaxial injectors show minor differences in their geometric dimensions but the same design concept was applied for both injectors.

Table 1 Specifications of biliquid swirl coaxial injectors adopted for two injector heads

Inj. Head	Inj. Layout	No. of Inj.	$d_{t,f}$, mm	$d_{t,o}$, mm	$d_{s,f}$, mm	$d_{s,o}$, mm	d_{oo}, mm	$d_{n,f,}$ mm	$d_{n,o}$, mm	n_f	n_o	$\dot{m}_{inj}$, kg/s
A	Concentric	19	1.25	1.05	8.0	5.5	4.6	8.0	3.0	6	4	0.232
B	Equidistant	13	1.50	1.00	10.0	6.8	5.5	10.0	3.9	6	6	0.338

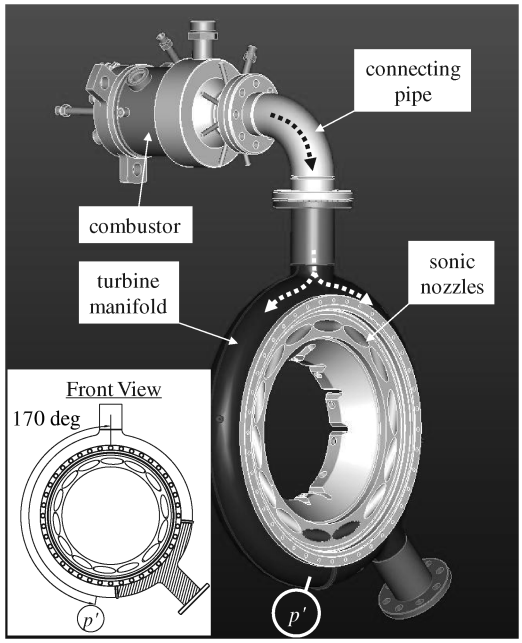

Fig. 4 Three-dimensional model of an assembly of a combustor and a turbine manifold for simulating combustion conditions in a powerpack.

B. Chamber Hardware

The combustion chamber adopted an active cooling method, that is, regenerative cooling was used as depicted in Fig. 2. The regenerative combustion chamber has cooling channels on the cylindrical inner wall enclosed by an outer stainless steel wall [13]. A gas generator in an LRE system can be pressurized by choking a combustion gas flow exiting into a turbine; thus, stand-alone combustion tests of an experimental fuel-rich combustor require a device simulating a turbine inlet sonic condition. In this study, two different types of a nozzle device have been used to operate the combustors at elevated pressures in the vicinity of 5.0 MPa. The first one is a short nozzle seen in Fig. 2, and the second one is a turbine manifold with a connecting pipe as presented in Fig. 4. The turbine manifold has a broken doughnutlike shape with 11 sonic nozzles.

C. Experimental Procedure

A series of combustion tests listed in Table 2 were conducted. The chamber pressure was varied from 4.10 ($p_c/p_{\mathrm{cr,o}} = 0.81$) to 7.24 MPa ($p_c/p_{\mathrm{cr,o}} = 1.44$), covering subcritical to supercritical oxygen pressures at a mixture ratio in the vicinity of 0.32. The critical pressures and temperatures of oxygen and Jet A-1 are 5.043 MPa and 154.6 K [14] and 2.33 MPa and 683 K [15], respectively.

Propellant supplies to the combustors were achieved through constant pressurization of run tanks using high-pressure gaseous nitrogen, and mass flow rates were measured using a serial combination of one Coriolis mass flow meter (Micromotion) and two turbine flow meters (Hoffer) installed on each propellant line. All the valve opening and closing sequences of the test facility during the combustion tests were automatically controlled by a preset programmable logic controller (Allen Bradley). The ignition in the chamber was achieved by using a gaseous methane/oxygen torch flame introduced into the inside of the chamber through a port on the chamber cylindrical wall. A steady condition at a constant static chamber pressure usually lasted for 5 s for all the tests.

Static properties like pressure and temperature across the combustor were simultaneously measured, and pressure fluctuations were also measured at the injector manifolds, the chamber, and the turbine manifold as specified in Figs. 2 and 4. Their signals were stored for postanalysis. An oxidizer dynamic sensor (PCB Piezotronics, 102A11) and a fuel dynamic sensor (PCB Piezotronics, 101A04) had to be installed with an extension tube due to space limitations. Because wave speeds in kerosene and LOx at a nominal operating condition are estimated at around 1100 and 643 m/s, respectively, time delays due to the extension become less than 0.06 ms and can be regarded as negligible for the present analysis. A helium-bleed, water-cooled piezoelectric dynamic pressure transducer (PCB Piezotronics, 123A24) was flush mounted on the combustor cylinder wall at an axial location 40 mm away from the injector faceplate. Another one was mounted on the long side of the turbine manifold as depicted in Fig. 4. Dynamic properties like pressure fluctuations were simultaneously sampled at 25 or 50 kHz using a high-frequency data acquisition system (Nicolet, Odyssey) and static properties at 100 Hz using a separate data acquisition system (National Instrument, PCI).

The characteristic velocities of the combustors used in the present study are presented in Fig. 5. An increase of characteristic velocities along with a mixture ratio ranging from 0.25 to 0.35 very closely matches the published, experimental results from LOx/RP-1 fuel-rich combustion [16]. In that all the results were acquired from the combustion of heavy hydrocarbon, they may show a small discrepancy in a characteristic velocity due to a difference in heating value. It becomes obvious that the mixture ratio is the dominant factor determining a characteristic velocity at fuel-rich conditions regardless of the combustion pressure, and the results ensure that the combustors reveal the inherent features of fuel-rich combustion.

III. Results and Discussion

A. Injector Head Configuration

The experiments for the comparison of the effects of injector head configuration were conducted using a combustor with a short nozzle installed (see Fig. 2). To understand the dynamic characteristics of

Table 2 Test conditions of the present study

Test No.	Inj. Head	Nozzle	$\dot{m}_f$, kg/s	$\dot{m}_o$, kg/s	p_c, MPa	Mixture ratio	T_f, K	T_o, K	$\Delta p_{\mathrm{inj},f}$, MPa	$\Delta p_{\mathrm{inj,o}}$, MPa
1	A	Short	3.26	1.09	5.96	0.34	303	114	1.03	0.974
2	A	Short	3.82	1.18	6.47	0.31	303	108	1.39	1.07
3	A	Short	2.82	0.86	4.75	0.30	301	118	0.775	0.644
4	A	Short	3.92	1.28	6.98	0.33	301	111	1.46	1.34
5	B	Short	3.40	1.04	5.70	0.31	305	120	1.16	1.43
6	B	Short	3.59	1.18	6.49	0.33	305	115	1.28	1.61
7	B	Short	2.90	0.86	4.63	0.30	304	125	0.830	1.08
8	B	Short	3.80	1.30	7.24	0.34	303	119	1.45	1.93
9	A	TM	3.50	1.15	5.43	0.33	296	114	1.24	1.34
10	A	TM	3.92	1.22	5.91	0.31	295	115	1.54	1.56
11	A	TM	2.61	0.88	4.23	0.34	292	120	0.810	0.819
12	A	TM	3.03	0.97	4.46	0.32	291	119	0.945	0.892
13	A	TM	3.18	1.07	5.16	0.34	290	115	1.03	1.22
14	A	TM	3.16	1.07	5.12	0.34	290	126	1.06	1.23
15	A	TM	2.78	0.90	4.27	0.32	290	121	0.815	0.854
16	A	TM	2.86	0.86	4.10	0.30	286	123	——	——
17	A	TM	3.04	0.96	4.68	0.32	290	126	0.965	0.992

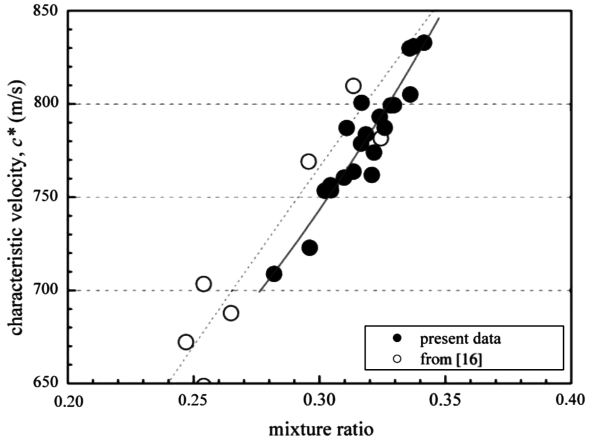

Fig. 5 Characteristic velocity variations as a function of a mixture ratio.

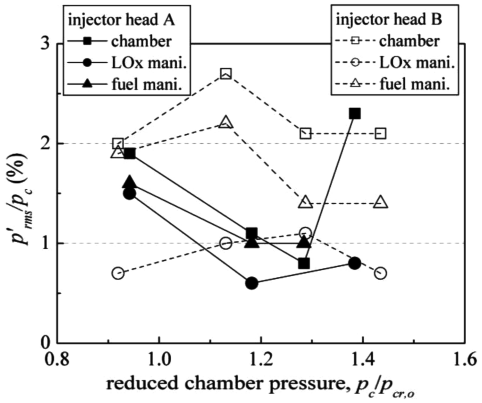

Fig. 6 Variations of normalized rms values of pressure fluctuations in the manifolds and the chamber for injector heads A and B as a function of a reduced chamber pressure.

fuel-rich combustion, pressure fluctuation measurements have been a major area of interest throughout the present study [17]. Acoustic intensity can be assessed by help of the estimation of rms values of pressure fluctuations. To eliminate dc drift from the measured signal, raw data were digitally filtered by a bandpass of 30–10,000 Hz. The rms values at each measurement location are normalized by their corresponding static pressures in Fig. 6. All the measurements indicate that combustion of the short nozzle combustor occurred in stable conditions with normalized rms values of less than 3%, which is regarded as satisfying the stability limit given by Klem and Fry [18]. Injector head A produces more sound combustion than injector head B over most of the conditions as shown in Fig. 6. The rms values of injector head A have minimums at a $p_c/p_{\mathrm{cr,o}}$ of 1.3, but injector head B shows a slight rise in rms value at a $p_c/p_{\mathrm{cr,o}}$ of 1.1 and it decreases along with the increase of static chamber pressure. The acoustic intensities for both injector heads reveal different patterns with static pressure, which implies that the combustion dynamic characteristics of both injector heads also show quite unique features originating from different configurations of swirl coaxial injectors and injector layouts.

Power spectral density plots of pressure fluctuations in the chamber for both injector heads are shown in Fig. 7. Frequency analysis of injector head A indicates there exist low-frequency pressure waves in the vicinity of 128 Hz for which the frequency gradually shifts up as chamber pressure increases. Also, for injector head B, a peak at a frequency of 127 Hz has been observed at a $p_c/p_{\mathrm{cr,o}}$ of 0.92. These kinds of low-frequency waves had also been observed in a similar study under a similar combustion environment [19]. These frequencies are far lower than the lowest value of the resonant mode frequencies of the chamber estimated as 1968 Hz for the first longitudinal mode.

The power of the low-frequency pressure waves attenuates as the chamber pressure increases for both cases of the injector heads. Injector head B shows more rapid attenuation of its low-frequency pressure wave than injector head A does even though the chamber acoustic intensity of injector head B is stronger than that of injector head A. This observation can be clarified by introducing the definition of a damping ratio, $\eta = (f_2 - f_1)/f_{\mathrm{peak}}$, where f_{peak} is a frequency at which a peak appears, and f_2 and f_1 are frequencies

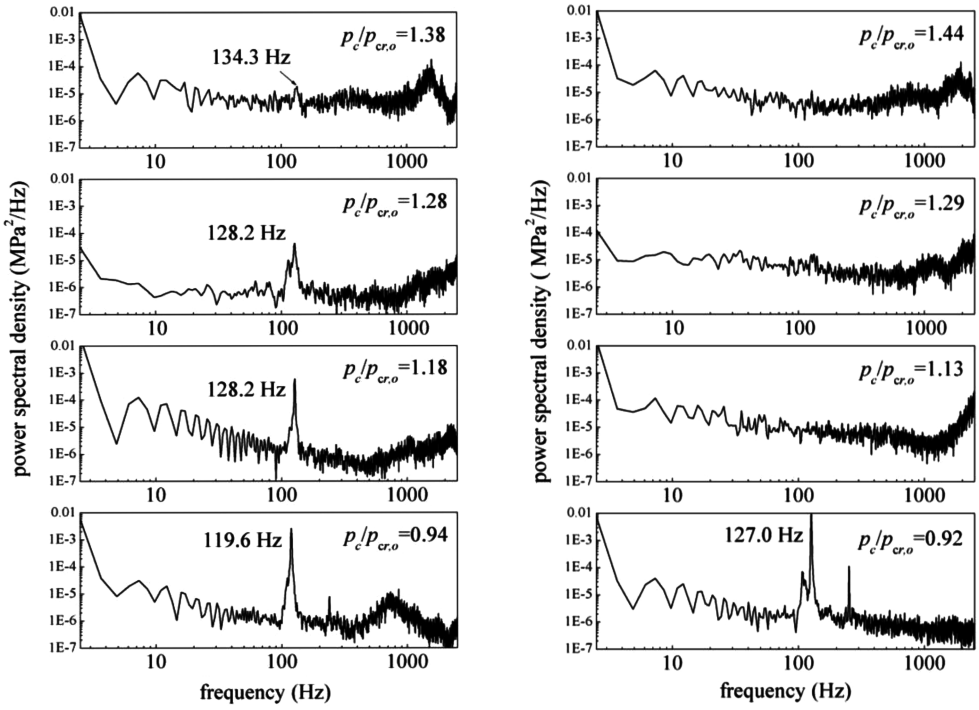

a) b)

Fig. 7 Power spectral density plots of combustion chamber pressure fluctuations at four different static chamber pressure conditions: a) injector head A, and b) injector head B.

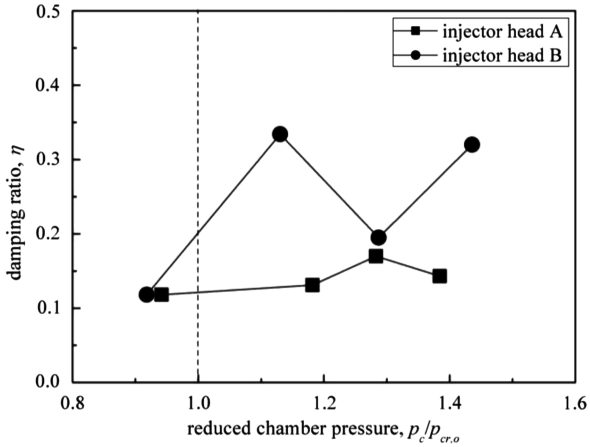

Fig. 8 Variations of a damping ratio for injector heads A and B as a function of a reduced chamber pressure.

corresponding to $1/\sqrt{2}$ times a peak amplitude with $f_2 > f_1$. A greater damping ratio indicates more attenuating characteristics of a pressure wave [20,21]. The estimation of a damping ratio for maximum peaks observed in the power spectrum plots of pressure fluctuation measurements shows that injector head B has more damping capability than injector head A (see Fig. 8). As expected in the power spectrum plots, the damping ratio increases with chamber pressure. It is interesting to observe that the damping ratios for both cases at chamber pressures under the oxygen critical pressure are estimated as very similar values. However, the damping ratio of injector head B becomes threefold at the supercritical chamber conditions, which results in the disappearance of the low-frequency wave. Injector head A just shows a slight increase in damping ratio even under the supercritical conditions.

A further understanding of the low-frequency wave sustained in the chamber can be obtained by phase analysis with the help of response functions between the manifold and the chamber pressure fluctuation measurements as presented in Fig. 9. A phase delay between the LOx manifold and the chamber might stay at approximately 10 deg for injector head A and 18 deg for injector head B. For the case of the fuel manifold and the chamber, there seem to be no phase delays with negligible values of −0.18 deg for injector head A and 3.2 deg for injector head B. Although error bounds for the estimation of a phase delay become wider as the pressure peak and the coherence between the measurements get weaker, it might be said that the phase delay between the manifolds and the chambers remains constant regardless of chamber pressure. From the results, it can be supposed that the relatively large phase delay between the LOx manifold and the chamber is due to the presence of the swirl chamber in the injector.

B. Swirling Motion

A swirl coaxial injector is known to have unique dynamic characteristics due to a swirling flow [22]. The hydraulic analysis of a swirl coaxial injector may provide a response function between injector pressure drop fluctuations and volume flow rate fluctuations as in the following equation;

$$\Pi_{\text{inj}} = \Pi_{\text{inj}}(f) = \frac{\mathbf{Q}'_{\text{inj}}}{\mathbf{Q}_{\text{inj}}} \Big/ \frac{\mathbf{\Delta p}'_{\text{inj}}}{\mathbf{\Delta p}_{\text{inj}}} = \frac{\Delta p_{\text{inj}}}{\Delta p_t} \cdot \frac{\Pi_t \Pi_n \Pi_s}{2\Pi_t \Pi_s + 1} \qquad (1)$$

where Π_t, Π_n, and Π_s are the transfer functions of a tangential entry, an injector nozzle, and a swirl chamber, respectively. The detailed descriptions of these functions can be found in [23]. The injector response function, Π_{inj}, consists of the effects from jet flow pulsation through tangential entries and from the swirling motion of flow in the swirl chamber. Estimated response functions of the LOx and the fuel parts of both injector heads are plotted in Fig. 10. The magnitudes of the response functions of the LOx parts become maximized at frequencies of 620 and 530 Hz for injector heads A and B,

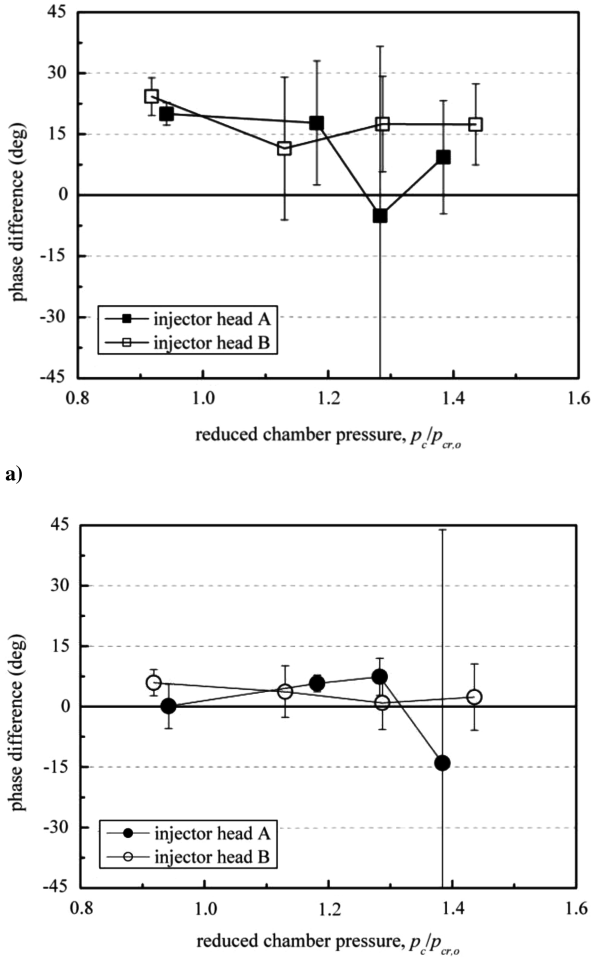

Fig. 9 Variations of a phase difference for injector heads A and B as a function of a reduced chamber pressure: a) the chamber and the LOx manifold, and b) the chamber and the fuel manifold.

respectively, although the magnitudes of the fuel part response functions gradually decrease with an increase of frequency without any maximal peaks.

From the results presented so far, the flow dynamics of the swirl coaxial injector under combustion can be described with the help of the sketch shown in Fig. 11. The hydraulic analysis implies that the internally mixed propellants out of an injector might pulsate with the largest amplitude at low frequencies with the maximum response values of the LOx part as shown in Fig. 10. The actual frequencies around 128 Hz observed in the combustion chamber result from the merging and disintegration of coherent structures emitted from the injector, which reveals their values are lower than those estimated in the hydraulic analysis. From the investigation of a swirl coaxial spray, it was observed that the wavelength between ligaments or droplet clusters increases as flow travels downstream. In the meantime, the spray velocity decreases away from an injector exit, which results in a decrease of droplet clusters' frequency along with an increase of axial distance [24]. The coherence of mixture inducing a heat release pulsation, which translates into pressure oscillations, becomes weaker as chamber pressure increases. The weakening of the mixture coherence seems to originate from the fact that the density gradient of LOx flow changes gradually at chamber pressures above the critical value of oxygen.

C. Chamber Configuration

According to the results from the stand-alone experiments, injector head A appears to be more vulnerable to periodic pressure fluctuations associated with a low-frequency pressure wave

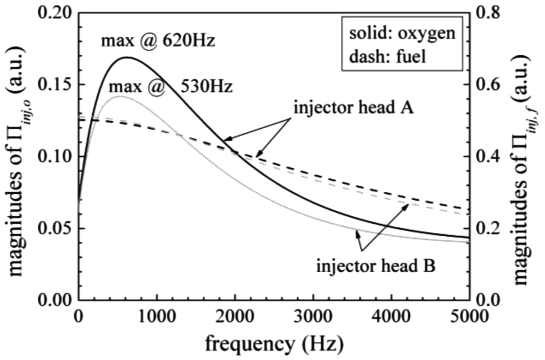

Fig. 10 Magnitudes of response functions of the LOx and the fuel parts of injector heads A and B as a function of frequency.

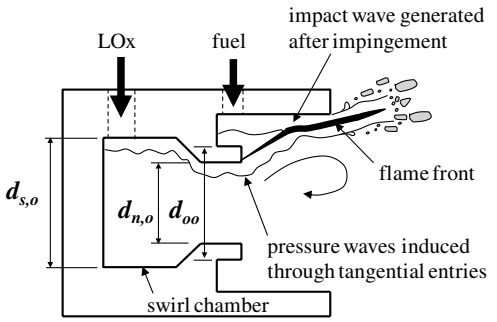

Fig. 11 Sketch of flow dynamics in a swirl coaxial injector.

sustained in the chamber. Dynamic characteristics of injector head A have been further investigated by conducting combustion tests using a connecting pipe and a turbine manifold nozzle (see Fig. 4). First, acoustic intensities by rms values of pressure fluctuations are plotted as a function of the chamber static pressure in Fig. 12. Spontaneous combustion instabilities occurred during combustion tests conducted at chamber pressures below 4.5 MPa ($p_c/p_{\mathrm{cr,o}} = 0.89$) as presented in Fig. 13. The onset times of combustion instabilities are 7.86, 7.2, 9.3, and 8.82 s for $p_c/p_{\mathrm{cr,o}}$ of 0.81, 0.84, 0.85, and 0.88, respectively. Spontaneously occurring combustion instabilities show well-known, chaotic characteristics regarding the timing of combustion instabilities. As seen in these figures, pressure fluctuation intensities double with the occurrence of unstable combustion. Without combustion instability, acoustic intensities in the chamber follow a linear relationship with respect to reduced chamber pressure, $0.125 p_c/p_{\mathrm{cr,o}}$,

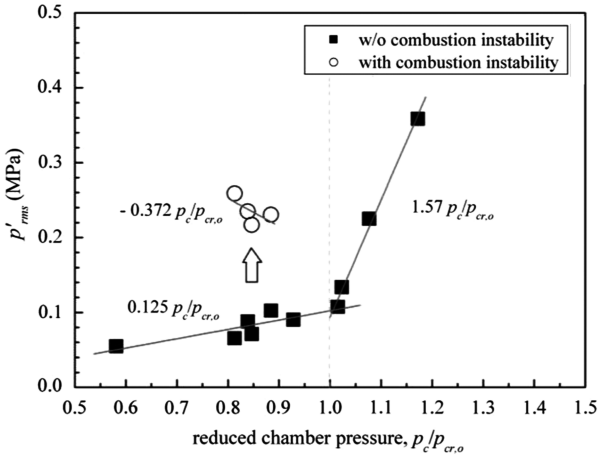

Fig. 12 Changes of rms values of pressure fluctuations in the chamber as a function of a reduced chamber pressure for injector head A assembled with the turbine manifold.

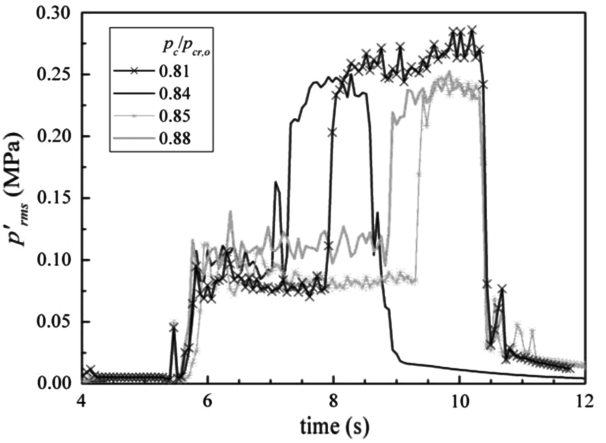

Fig. 13 Time traces of rms values of pressure fluctuations in the chamber when combustion instabilities occurred.

where 0.125 is the slope of change in p'_{rms}. Above a chamber pressure of 5.0 MPa, that is, the critical pressure of oxygen, pressure fluctuation intensity abruptly increases along with a reduced chamber pressure, at which no instability occurs. The gradient becomes steep up to 1.57, which is 10 times greater than that estimated below the critical pressure of oxygen. For unstable combustion conditions, rms intensities slowly attenuate as the chamber pressure approaches the critical pressure of oxygen.

Fast Fourier transform (FFT) analysis in Fig. 14 helps to understand the varying characteristics of pressure fluctuations in the chamber as a function of chamber pressure. At unstable combustion conditions, sharp peaks have been observed at a frequency of 330 Hz. These can still be regarded as low-frequency waves but they have a higher value than the pressure waves found in the combustor-alone tests. The second highest peaks have a frequency of twice the maximum peaks, which implies that the pressure wave is associated with the acoustic resonant modes of the chamber. This fact will be discussed in the following section. It is noteworthy that the pressure wave identified during the combustor-alone experiments at a frequency in the vicinity of 128 Hz does not appear anymore, whether the combustion is stable or not. This is due to the immediate

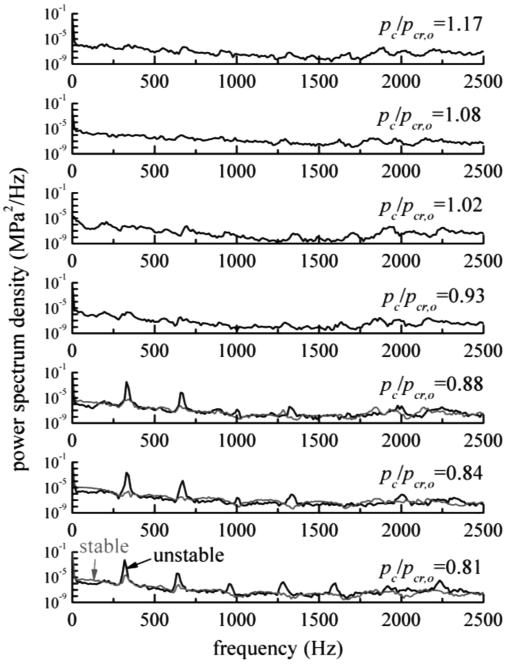

Fig. 14 Power spectrum density plots of pressure fluctuations in the chamber at various chamber static pressures for injector head A assembled with the turbine manifold.

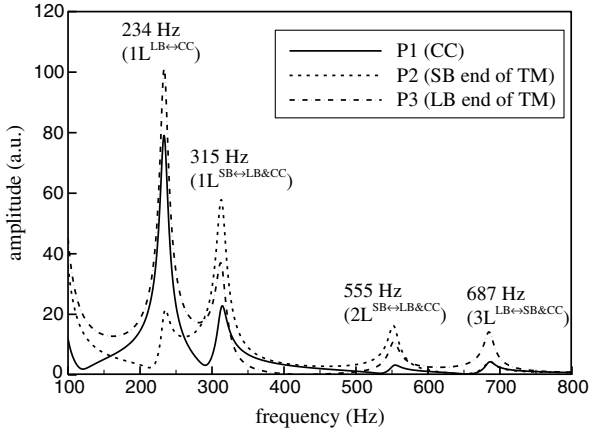

Fig. 15 Prediction of acoustic pressure response of the whole configuration with the actual turbine manifold.

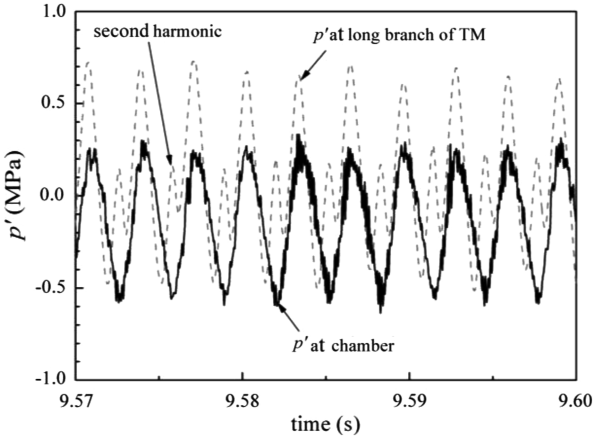

Fig. 17 Time traces of pressure fluctuations measured at the chamber and the long branch of the turbine manifold at the occurrence of combustion instability.

dissipation of pulsating coherent structures through the open end to the connecting pipe.

D. Linear Acoustic Analysis

In the full configuration with the actual turbine manifold as shown in Fig. 4, pressure fluctuations formed within the combustion chamber (CC) freely propagate through the connecting pipe to the turbine manifold (TM), which is acoustically closed at the nozzle throats due to choking. To identify the existing resonant modes of the whole system with complex geometry, in the present study, a three-dimensional analysis has been performed using an in-house acoustic solver for the Helmholtz equation in the frequency domain with a finite element method on unstructured grids. The details of the numerical method can be found elsewhere [25,26] and are not reported here. It is widely known that there exist significant departures from the chemical equilibrium state in extremely fuel-rich regimes for the hydrocarbon fuels, especially kerosene. Gas properties required for the acoustic analysis therefore, in this study, have been estimated based on a modified equilibrium calculation according to the procedure [27] used in the cycle simulation program (SEQ code) of the DLR, German Aerospace Research Center.

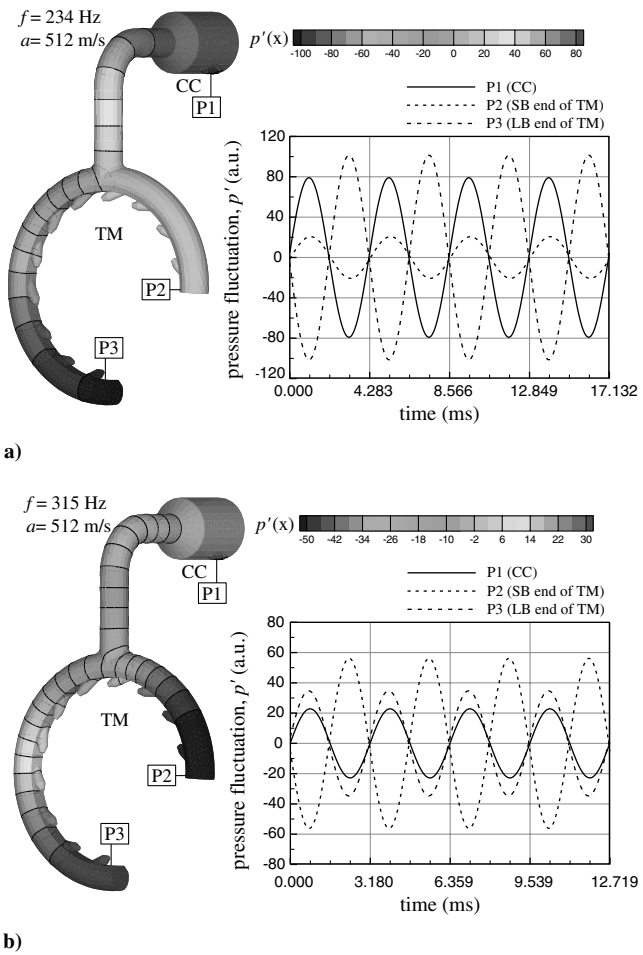

Fig. 16 Spatial modal shape and temporal signals of the longitudinal acoustic modes: a) 234 Hz, and b) 315 Hz.

Figure 15 presents the numerical results of linear acoustic response to external pressure excitation at a point with an infinitesimal magnitude over the frequency range of interest. In the low-frequency region in the vicinity of the experimentally observed one (330 Hz), there exist two different peaks that correspond to the first longitudinal resonant mode. At the resonant frequency of 234 Hz, the numerical results given in Fig. 16a show that the main acoustic mode is formed longitudinally between the combustion chamber and the long branch (LB) of the turbine manifold with a phase difference of 180 deg. At the resonant frequency of 315 Hz as seen in Fig. 16b, on the other hand, both of the injector plates of the combustor and the long branch end of the turbine manifold form the pressure antinodes with the same phase and resonate longitudinally with the short branch (SB), the end of which acts as another antinode with a phase difference of 180 deg. In terms of the phase delay, the latter prediction of Fig. 16b coincides with the experimental observation as plotted in Fig. 17. The discrepancy between the predicted frequency (315 Hz) and the measured one (330 Hz) is attributed mainly to uncertainty in the estimation of the sonic velocity of extremely fuel-rich combustion gas. As a consequence, the experimentally encountered combustion instabilities can be explained as acoustic coupling between the combustion response activated under a pressure lower than the oxygen critical pressure and the longitudinal resonant mode from the combustor to the short branch of the turbine manifold.

IV. Conclusions

The present research focuses on understanding the dynamic characteristics of fuel-rich combustion associated with variations of injector and chamber configuration. The combustion tests conducted with a short nozzle in the confined combustion chamber suggest that a swirl coaxial injector inherently bears a coherent mixture pulsating at a certain frequency. The oscillation frequencies are in the vicinity of 128 Hz estimated by an FFT analysis of the pressure fluctuation measurements. The hydraulic analysis indicates that volume flow rate fluctuations of oxygen may provide maximal responses at frequencies around 575 Hz, whereas the fuel part without a swirl chamber shows a gradual decrease of the response with frequency. The frequencies observed in the combustion chamber reveal lower values than the hydraulic analysis results due to the merging and

disintegration of coherent structures generated from the injector. The induced pressure wave attenuates along with the increase in chamber pressure and its damping characteristics are demarcated by the oxygen critical pressure in that injector head B shows the complete dissipation of the low-frequency wave whereas injector head A still maintains its wave even at chamber pressures above the oxygen critical pressure.

A series of combustion experiments has been conducted with the combustor connected to the turbine manifold and it showed that spontaneous, resonant combustion instabilities occurred at chamber pressures below 4.5 MPa ($p_c/p_{\mathrm{cr,o}} = 0.89$). Without combustion instability, acoustic intensities in the chamber follow a linear relationship with respect to a reduced chamber pressure, $0.125 p_c/p_{\mathrm{cr,o}}$. At conditions above the oxygen critical pressure, pressure fluctuation intensity abruptly increases with a gradient of 1.57 with respect to a reduced chamber pressure at which no instability occurs.

Three-dimensional acoustic analysis using an in-house solver for the Helmholtz equation shows that the injector faceplate and the long branch end of the turbine manifold form the pressure antinodes with the same phase and resonate longitudinally with the short branch, the end of which acts as another antinode having a phase difference of 180 deg. The numerical estimation of this resonant mode is 315 Hz, which corresponds to the experimental observation with a minor discrepancy due to uncertainty in the estimation of the sonic velocity of extremely fuel-rich combustion gas.

Swirl coaxial injectors under fuel-rich combustion show different combustion responses depending on their configuration and operating pressures, which results in different damping characteristics of hydraulic low-frequency fluctuations. The large response of the swirl coaxial injector operating below the oxygen critical pressure may trigger the longitudinal mode of spontaneous combustion instability.

Acknowledgment

The present study is a part of the Research and Development of Korea Space Launch Vehicle-I project financially supported by the Ministry of Education, Science and Technology (MEST); the authors would like to thank the MEST for its support.

References

[1] Zehetner, H. C., "Liquid Propellant Gas Generators," NASA SP-8081, 1972.

[2] Huzel, D. K., and Huang, D. H., *Modern Engineering for Design of Liquid-Propellant Rocket Engines*, Progress in Aeronautics and Astronautics, Vol. 147, AIAA, Washington, DC, 1992, p. 118.

[3] Dennis, H. J., Jr., and Sanders. T., "NASA Fastrac Engine Gas Generator Component Test Program and Results," AIAA Paper 2000-3401, 2000.

[4] Nesman, T., and Dennis, J., "Fastrac Gas Generator Testing," *Tenth Thermal and Fluids Analysis Workshop*, NASA Marshall Space Flight Center Rept. 19990105709, Sept. 1999.

[5] Heubner, A. W., "High Pressure LOx/Hydrocarbon Preburner Injector Investigation," AIAA Paper 2982-1152, 1982.

[6] Mah, C. S., "Evaluating the Operational Limits of a Gas Generator," AIAA Paper 2001-3990, 2001.

[7] Zurbach, S., Thomas, J. L., Verplancke, C., Vingert, L., and Habiballah, M., "LOx/Methane Studies for Fuel Rich Preburner," AIAA Paper 2003-5063, 2003.

[8] Fournet, A., Lonchard, J. M., and Thomas, J. L., "Technological Demonstration for Low Cost Gas Generator," AIAA Paper 2004-4006, 2004.

[9] Gill, G. S., and Nurick, W. H., "Liquid Rocket Engine Injectors," NASA SP-8089, 1976.

[10] Sivakumar, D., and Raghunandan, B. N., "Role of Geometric Parameters on the Drop Size Characteristics of Liquid-Liquid Coaxial Swirl Atomizers," *Atomization and Sprays*, Vol. 8, 1998, pp. 547–563.

[11] Soltani, M. R., Ghorbanian, K., Ashjaee, M., and Morad, M. R., "Spray Characteristics of a Liquid-Liquid Coaxial Swirl Atomizer at Different Mass Flow Rates," *Aerospace Science and Technology*, Vol. 9, 2005, pp. 592–604.
doi:10.1016/j.ast.2005.04.004

[12] Kim, D., Han, P., Im, J.-H., Yoon, Y., and Bazarov, V. G., "Effect of Recess on the Spray Characteristics of Liquid-Liquid Swirl Coaxial Injectors," *Journal of Propulsion and Power*, Vol. 23, No. 6, 2007, pp. 1194–1203.
doi:10.2514/1.30450

[13] Seo, S., Ahn, K., Han, Y.-M., Ryu, C.-S., and Kim, H.-J., "Design and Manufacture of Regenerative Cooling Fuel-Rich Gas Generators," Korea Aerospace Research Inst., KARI-CCT-TM-2006-03, 2006.

[14] Sychev, V. V., Vasserman, A. A., Kozlov, A. D., Spiridonov, G. A., and Tsymarny, V. A., *Thermodynamic Properties of Oxygen*, Hemisphere, Washington, DC, 1987, p. 93.

[15] Edwards, T., "Liquid Fuels and Propellants for Aerospace Propulsion: 1903-2003," *Journal of Propulsion and Power*, Vol. 19, No. 6, 2003, pp. 1089–1107.
doi:10.2514/2.6946

[16] Lawver, B. R., "Test Verification of LOx/RP-1 High-Pressure Fuel/Oxidizer-Rich Preburner Designs," AIAA Paper 1982-1153, 1982.

[17] Dranovsky, M. L., *Combustion Instabilities in Liquid Rocket Engines: Testing and Development Practices in Russia*, Vol. 221, Progress in Astronautics and Aeronautics, edited by V. Yang, F. E. C. Culick, and D. G. Talley, AIAA, Washington, DC, 2007.

[18] Klem, M. D., and Fry, R. S., "Guidelines for Combustion Stability Specifications and Verification Procedures for Liquid Propellant Rocket Engines," Johns Hopkins Univ. Chemical Propulsion Information Agency, Rept. 655, Silver Spring, MD, 1997.

[19] Seo, S., Lee, K.-J., Han, Y.-M., Kim, S.-H., Kim, J.-G., Moon, I.-Y., and Seol, W.-S., "Study on Combustion Characteristics of Unielement Thrust Chambers with Various Injectors," *Journal of the Korean Society of Propulsion Engineers*, Vol. 8, 2004, pp. 85–94.

[20] Harrje, D. T., and Reardon, F. H. (eds.), "Liquid Propellant Rocket Combustion Instability," NASA SP-194, 1972.

[21] Yang, V., and Anderson, W. E. (eds.), *Liquid Rocket Engine Combustion Instability*, Vol. 169, Progress in Astronautics and Aeronautics, AIAA, Washington, DC, 1995.

[22] Bazarov, V. G., and Yang, V., "Liquid-Propellant Rocket Engine Injector Dynamics," *Journal of Propulsion and Power*, Vol. 14, No. 5, 1998, pp. 797–806.
doi:10.2514/2.5343

[23] Bazarov, V., Yang, V., and Puri, P., "Design and Dynamics of Jet and Swirl Injectors," *Liquid Rocket Thrust Chambers: Aspects of Modeling, Analysis, and Design*, edited by V. Yang, M. Habiballah, J. Hulka, and M. Popp, Vol. 200, Progress in Astronautics and Aeronautics, AIAA, Reston, VA, 2004. pp. 19–103.

[24] Rhys, N. O., Moser, M., and Eskridge, R. H., "Unsteady Breakup of a Swirl Coaxial Injector," AIAA Paper 1997-2844, 1997.

[25] Kim, S.-K., Kim, H. J., Seol, W., and Sohn, C. H., "Acoustic Stability Analysis of Liquid Propellant Rocket Combustion Chambers," AIAA Paper 2004-4142, 2004.

[26] Sohn, C. H., Park, I-S., Kim, S.-K., and Kim, H. J., "Acoustic Tuning of Gas-Liquid Scheme Injectors for Acoustic Damping in a Combustion Chamber of a Liquid Rocket Engine," *Journal of Sound and Vibration*, Vol. 304 Nos. 3–5, 2007, pp. 793–810.
doi:10.1016/j.jsv.2007.03.036

[27] Kauffmann, J., Herbertz, A., and Sippel, M., "Systems Analysis of a High Thrust, Low-Cost Rocket Engine," *International Conference on Green Propellant for Space Propulsion*, European Space Research and Technology Centre, Noordwijk, The Netherlands, June 2001.

D. Talley
Associate Editor